

# Enhancement-Mode Atomic-Layer-Deposited $\text{In}_2\text{O}_3$ Transistors With Maximum Drain Current of 2.2 A/mm at Drain Voltage of 0.7 V by Low-Temperature Annealing and Stability in Hydrogen Environment

Mengwei Si<sup>ID</sup>, Adam Charnas<sup>ID</sup>, Zehao Lin, and Peide D. Ye<sup>ID</sup>, *Fellow, IEEE*

**Abstract**—In this article, we demonstrate atomic-layer-deposited (ALD) indium oxide ( $\text{In}_2\text{O}_3$ ) transistors with a record high drain current of 2.2 A/mm at  $V_{DS}$  of 0.7 V among oxide semiconductor transistors with the enhancement-mode operation. The impact of back-end-of-line (BEOL) compatible low-temperature annealing is systematically studied on these highly scaled  $\text{In}_2\text{O}_3$  transistors with channel length ( $L_{ch}$ ) down to 40 nm, channel thickness ( $T_{ch}$ ) down to 1.2 nm, and equivalent oxide thickness (EOTs) of 2.1 nm, at annealing temperatures from 250 °C to 350 °C in  $\text{N}_2$ ,  $\text{O}_2$ , and forming gas (FG, 96%  $\text{N}_2/4\%$   $\text{H}_2$ ) environments. Annealing in all different environments is found to significantly improve the performance of ALD  $\text{In}_2\text{O}_3$  transistors, resulting in enhancement-mode operation, high mobility, reduced bulk and interface trap density ( $D_{it}$  as low as  $6.3 \times 10^{11} \text{ cm}^{-2} \cdot \text{eV}^{-1}$ ), and nearly ideal subthreshold slope (SS) of 63.8 mV/dec. Remarkably, the ALD  $\text{In}_2\text{O}_3$  devices are found to be stable in hydrogen environment, being less affected by the well-known hydrogen doping issue in indium–gallium–tin-oxide (IGZO). Therefore, low-temperature ALD  $\text{In}_2\text{O}_3$  transistors are highly compatible with the hydrogen-rich environment in BEOL fabrication processes.

**Index Terms**—Annealing, atomic layer deposition (ALD), back-end-of-line (BEOL) compatible, hydrogen, indium oxide, oxide semiconductor, thin-film transistor.

## I. INTRODUCTION

OXIDE semiconductors are widely employed in thin-film transistors [1], [2] and are promising channel materials

Manuscript received December 14, 2020; accepted January 17, 2021. Date of publication January 29, 2021; date of current version February 24, 2021. This work was supported in part by the Semiconductor Research Corporation (SRC) nCore Innovative Materials and Processes for Accelerated Compute Technologies (IMPACT) Center and in part by the Air Force Office of Scientific Research (AFOSR) and SRC/Defense Advanced Research Projects Agency (DARPA) Joint University Microelectronics Program (JUMP) Applications and Systems-driven Center for Energy-Efficient integrated Nano Technologies (ASCENT) Center. The review of this article was arranged by Editor J. F. Conley. (Corresponding author: Peide D. Ye.)

The authors are with the Birk Nanotechnology Center, School of Electrical and Computer Engineering, Purdue University, West Lafayette, IN 47907 USA (e-mail: yep@purdue.edu).

Color versions of one or more figures in this article are available at <https://doi.org/10.1109/TED.2021.3053229>.

Digital Object Identifier 10.1109/TED.2021.3053229

for complementary metal–oxide–semiconductor (CMOS) back-end-of-line (BEOL) compatible transistors for monolithic (3-D) integration. Indium oxide ( $\text{In}_2\text{O}_3$ ) [3], [4] or doped- $\text{In}_2\text{O}_3$  [5]–[10] are being investigated due to their low thermal budget growth and fabrication, high mobility, atomically smooth surface, and wafer-scale homogenous films. The capability of atomic layer deposition (ALD) to deposit atomically thin and conformal  $\text{In}_2\text{O}_3$  films on 3-D structures enables tremendous new opportunities toward 3-D device integration [3], [4], [11]–[14]. High-performance scaled  $\text{In}_2\text{O}_3$  transistors by ALD have been demonstrated with maximum drain current ( $I_{D,max}$ ) exceeding 2.0 A/mm at depletion-mode operation [4]. Enhancement-mode operation with threshold voltage ( $V_T$ ) above zero was also achieved by decreasing channel thickness ( $T_{ch}$ ) down to 0.7 and 1 nm by the accurate thickness control of ALD, but also causes the reduction of channel mobility and  $I_{D,max}$  down to 1.0 A/mm [3], [4]. Such phenomenon was understood by the impact of quantum confinement on the trap neutral level (TNL) alignment, confirmed by both experiments and *ab initio* density functional theory (DFT) simulation [3].

Meanwhile, stability in hydrogen-rich environment is required and crucial for BEOL compatible process because  $\text{H}_2$  is the byproduct during BEOL fabrication [15]. Post-deposition hydrogen doping to amorphous indium–gallium–tin-oxide (IGZO), such as  $\text{N}_2/\text{H}_2$  annealing and H plasma treatment, was well understood to always increase free electron density up to  $\sim 10^{20} / \text{cm}^3$  [16]–[18]. Hydrogen was understood as shallow donor and to form an OH group [17]. Therefore, whether  $\text{In}_2\text{O}_3$  or doped  $\text{In}_2\text{O}_3$  can be stable in the CMOS BEOL process becomes a serious concern.

In this article, the impact of post-deposition annealing in various environments, such as  $\text{O}_2$ ,  $\text{N}_2$ , and forming gas (FG, 96%  $\text{N}_2/4\%$   $\text{H}_2$ ), at various BEOL compatible low temperatures from 250 °C to 350 °C on ALD  $\text{In}_2\text{O}_3$  transistors are systematically studied. Annealing in all different environments is found to shift the  $V_T$  positively and lead to the enhancement-mode operation, where the physical origin is speculated as the annihilation of oxygen vacancies by excessive oxygen in the as-deposited films. Remarkably,

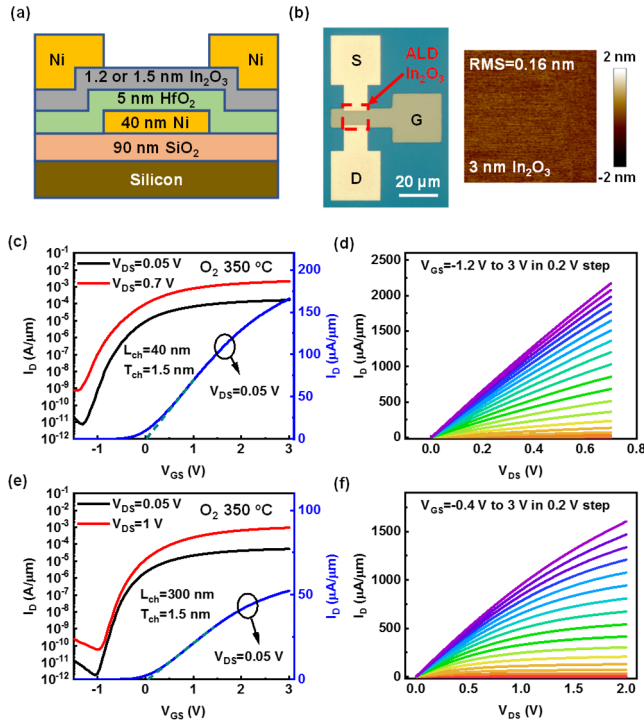


**Fig. 1.** (a) Schematic and (b) photo image of an  $\text{In}_2\text{O}_3$  transistor and AFM measurement of the surface roughness on a 3-nm as-deposited ALD  $\text{In}_2\text{O}_3$  film. (c)  $I_D$ - $V_{GS}$  and (d)  $I_D$ - $V_{DS}$  characteristics of an  $\text{In}_2\text{O}_3$  transistor with  $L_{ch}$  of 40 nm,  $T_{ch}$  of 1.5 nm, and annealed at 350 °C in  $\text{O}_2$ . (e)  $I_D$ - $V_{GS}$  and (f)  $I_D$ - $V_{DS}$  characteristics of an  $\text{In}_2\text{O}_3$  transistor with  $L_{ch}$  of 300 nm,  $T_{ch}$  of 1.5 nm, and annealed at 350 °C in  $\text{O}_2$ .

the ALD  $\text{In}_2\text{O}_3$  devices are found to be stable in hydrogen environment, being less affected by the well-known hydrogen doping issue in IGZO [16]–[18]. Therefore, ALD  $\text{In}_2\text{O}_3$  could be highly compatible with hydrogen-rich environment in CMOS BEOL fabrication processes.

High-performance ALD enhancement-mode  $\text{In}_2\text{O}_3$  transistors are also demonstrated by the optimized post-deposition annealing. Record high drain current of 2.2 A/mm at  $V_{DS}$  of 0.7 V with  $V_T$  of 0.02 V is achieved on this enhancement-mode  $\text{In}_2\text{O}_3$  transistor with channel length ( $L_{ch}$ ) of 40 nm, channel thickness ( $T_{ch}$ ) of 1.5 nm, and equivalent oxide thickness (EOTs) of 2.1 nm, with 350 °C annealing in  $\text{O}_2$ . A detailed benchmarking information of the maximum drain currents among oxide semiconductors-based transistors can be found in [5]. A high field-effect mobility ( $\mu_{FE}$ ) of 91.0  $\text{cm}^2/\text{V}\cdot\text{s}$  is achieved. High drain current over 1.0 A/mm is also achieved on enhancement-mode  $\text{In}_2\text{O}_3$  transistors with  $L_{ch}$  of 40 nm,  $T_{ch}$  of 1.2 nm, and EOT of 2.1 nm, with low-temperature annealing in  $\text{O}_2$ ,  $\text{N}_2$ , and FG. Subthreshold slope (SS) as low as 63.8 mV/dec is obtained on  $\text{In}_2\text{O}_3$  transistors with FG annealing, corresponding to an interface trap density ( $D_{it}$ ) of  $6.3 \times 10^{11} \text{ cm}^{-2}\cdot\text{eV}^{-1}$ , indicating FG annealing can effectively passivate the interface trap states at  $\text{HfO}_2/\text{In}_2\text{O}_3$  oxide/oxide interface.

## II. EXPERIMENTS

**Fig. 1(a)** illustrates the schematic of an  $\text{In}_2\text{O}_3$  transistor, employing the same structure as previously reported in [4].

The gate-stack includes 40-nm Ni as gate metal, 5-nm  $\text{HfO}_2$  as gate dielectric, 1.2 and 1.5 nm  $\text{In}_2\text{O}_3$  as semiconducting channels, and 80 nm Ni as source/drain electrodes. **Fig. 1(b)** presents the photo image of a typical fabricated device.

The device fabrication process is similar to [4]. The device fabrication starts with standard cleaning of p+ Si substrate with 90 nm thermally grown  $\text{SiO}_2$ . 90-nm  $\text{SiO}_2$  is used for device isolation. A bi-layer photoresist lithography process (Polymethylglutarimide (PMGI) + AZ1518) was then applied for the sharp lift-off of 40-nm Ni gate metal by e-beam evaporation. Then, 5-nm  $\text{HfO}_2$  was deposited by ALD at 200 °C, using  $[(\text{CH}_3)_2\text{N}]_4\text{Hf}$  (TDMAHf) and  $\text{H}_2\text{O}$  as Hf and O precursors. 1.2 and 1.5-nm thick  $\text{In}_2\text{O}_3$  films were then deposited by ALD at 225 °C, using  $(\text{CH}_3)_3\text{In}$  (TMIn) and  $\text{H}_2\text{O}$  as In and O precursors.  $\text{N}_2$  is used as the carrier gas. ALD  $\text{In}_2\text{O}_3$  film has a low surface roughness, as shown in **Fig. 1(b)**, where 3-nm as-deposited  $\text{In}_2\text{O}_3$  on Si substrate has a surface roughness of 0.16 nm, measured by atomic force microscopy (AFM), indicating ALD  $\text{In}_2\text{O}_3$  film is atomically smooth. As-deposited ALD  $\text{In}_2\text{O}_3$  is amorphous [4], further material studies are needed to determine whether annealing at high temperatures changes the phase of ALD  $\text{In}_2\text{O}_3$ . The ALD deposition process may introduce both excessive hydrogen and oxygen into the  $\text{In}_2\text{O}_3$  film from the water precursor. The ALD temperature at 225 °C may be insufficient to passivate all oxygen deficiencies. Channel isolation was done by wet etching of  $\text{In}_2\text{O}_3$  using concentrated hydrochloric acid. Hydrochloric acid is another possible hydrogen source. 80-nm Ni was then deposited by e-beam evaporation as S/D contacts, patterned by electron beam lithography, with a minimum  $L_{ch}$  of 40 nm. The fabricated devices were annealed in  $\text{O}_2$ ,  $\text{N}_2$ , or FG for 30 s at different temperatures from 250 °C to 350 °C. Note that the fabrication process may introduce defects into the  $\text{In}_2\text{O}_3$  channel since it is just nanometer thin, causing a  $L_{ch}$  dependent carrier density and  $V_T$ , which can be completely removed by annealing. This will be discussed in detail in Section III.

## III. RESULTS AND DISCUSSION

**Fig. 1(c)** and **(d)** presents the representative  $I_D$ - $V_{GS}$  and  $I_D$ - $V_{DS}$  characteristics of an  $\text{In}_2\text{O}_3$  transistor with  $L_{ch}$  of 40 nm and  $T_{ch}$  of 1.5 nm with 350 °C annealing in  $\text{O}_2$ . Maximum  $I_D$  of 2.2 A/mm is achieved at a low  $V_{DS}$  of 0.7 V with  $V_T$  of 0.02 V. Here, enhancement-mode is  $V_T > 0$  V by definition. Note that although  $V_T > 0$  V is achieved, a relatively large current at  $V_{GS} = 0$  V is still existing, indicating that larger  $V_T$  is still needed to achieve low off-current at  $V_{GS} = 0$  V. A low ON-resistance ( $R_{on}$ ) of 0.32  $\Omega\cdot\text{mm}$  is obtained, suggesting a very low contact resistance ( $R_C$ ). **Fig. 1(e)** and **(f)** presents the  $I_D$ - $V_{GS}$  and  $I_D$ - $V_{DS}$  characteristics of an  $\text{In}_2\text{O}_3$  transistor with  $L_{ch}$  of 300 nm and  $T_{ch}$  of 1.5 nm, showing well-behaved  $I_D$  saturation at high  $V_{DS}$  greater than  $V_{GS}-V_T$ .

**Fig. 2** summarizes the scaling metrics of  $\text{In}_2\text{O}_3$  transistors with  $L_{ch}$  from 0.8  $\mu\text{m}$  down to 40 nm and with  $T_{ch}$  of 1.5 nm. The devices with and without  $\text{O}_2$  annealing at 350 °C are compared. Each data point represents the average of at least 5 devices. The small error bar in these plots demonstrates

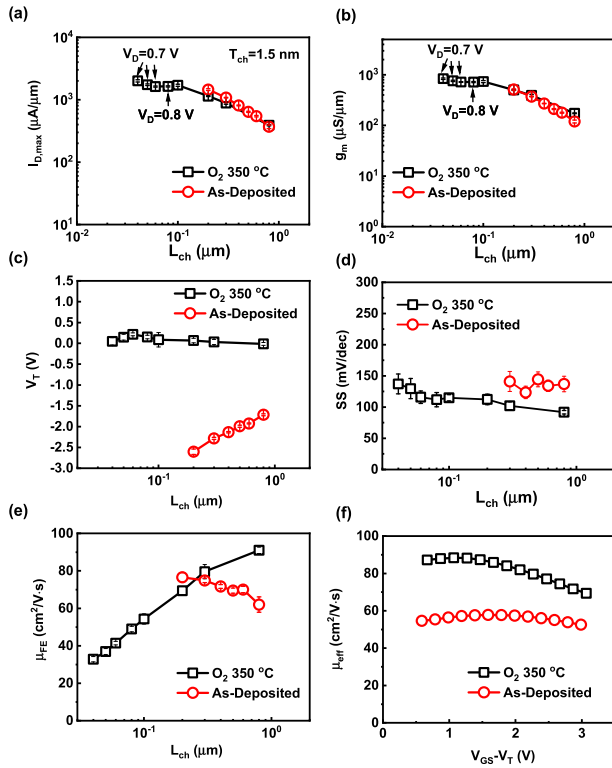


**Fig. 2.** (a)  $I_{D,max}$ , (b)  $g_m$ , (c)  $V_T$ , (d) SS, and (e)  $\mu_{FE}$  scaling metrics of  $\text{In}_2\text{O}_3$  transistors with  $L_{ch}$  from 0.8  $\mu\text{m}$  to 40 nm and  $T_{ch}$  of 1.5 nm. Each data point represents the average of at least 5 devices. The data are from devices with and without 350 °C annealing in O<sub>2</sub>. (f) Effective mobility versus  $V_{GS} - V_T$  extracted from a device with  $L_{ch}$  of 0.8  $\mu\text{m}$  and  $T_{ch}$  of 1.5 nm with 350 °C O<sub>2</sub> annealing and from a device with  $L_{ch}$  of 1  $\mu\text{m}$  and  $T_{ch}$  of 1.5 nm with as-deposited film.  $I_{D,max}$  and  $g_m$  are extracted at  $V_{DS} = 1$  V unless otherwise specified.

that the ALD-based  $\text{In}_2\text{O}_3$  transistors are highly uniform. Fig. 2(a) and (b) shows the  $I_{D,max}$  and transconductance ( $g_m$ ) versus  $L_{ch}$  characteristics.  $I_{D,max}$  and  $g_m$  are extracted at  $V_{DS} = 1$  V unless otherwise specified. A high average  $I_{D,max} > 2.0$  A/mm at  $V_{DS}$  of 0.7 V is achieved. Low drain voltages are used at shorter channels to avoid the impact of self-heating effect. Fig. 2(c) studies the impact of O<sub>2</sub> annealing on  $V_T$ , showing a large positive  $V_T$  shift by 350 °C annealing in O<sub>2</sub>. Note that the as-deposited  $\text{In}_2\text{O}_3$  transistors have a clearly  $L_{ch}$  dependent  $V_T$  even in long channel devices while  $V_T$  has negligible  $L_{ch}$  dependence after O<sub>2</sub> annealing, suggests such  $V_T$  dependence is from the defects introduced during device fabrication and these defects are completely removed by O<sub>2</sub> annealing, such phenomenon is further confirmed by detailed N<sub>2</sub>/O<sub>2</sub>/FG annealing completely studies in Figs. 4–6. Fig. 2(d) presents the SS versus  $L_{ch}$  characteristics at  $V_{DS}$  of 0.05 V. Minimum SS of 91.7 mV/dec is achieved. Fig. 2(e) shows the scaling metrics on  $\mu_{FE}$ .  $\mu_{FE}$  is extracted from extrinsic maximum  $g_m$  at low  $V_{DS}$  of 0.05 V. High  $\mu_{FE}$  of 91.0  $\text{cm}^2/\text{V}\cdot\text{s}$  is achieved at ultrathin  $T_{ch}$  of 1.5 nm, which is rather high among amorphous oxide semiconductors, being benefitted from the atomically smooth surface by ALD, which is also consistent with extracted effective mobility ( $\mu_{eff}$ ) as shown in Fig. 2(f). Note that the extracted extrinsic mobilities are still under-estimated without considering the

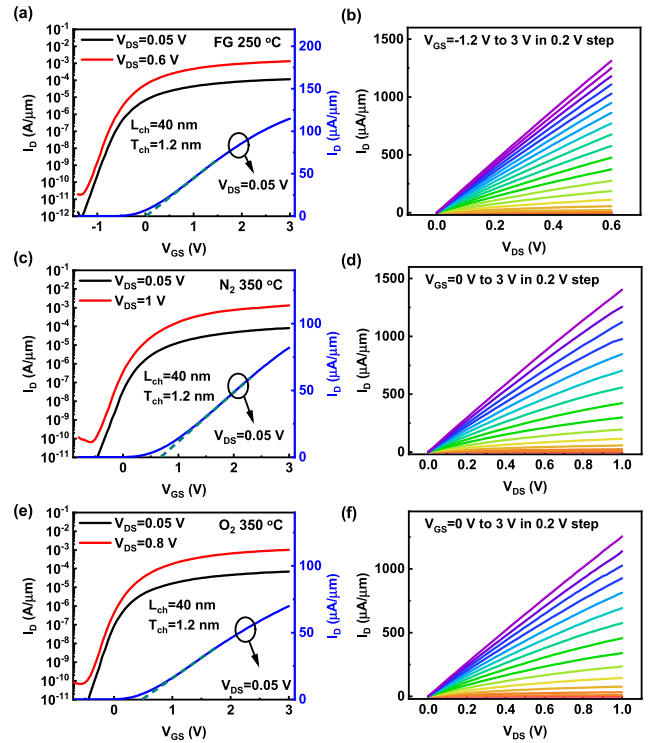


**Fig. 3.** (a)  $I_D - V_{GS}$  and (b)  $I_D - V_{DS}$  characteristics of an  $\text{In}_2\text{O}_3$  transistor with  $L_{ch}$  of 40 nm and  $T_{ch}$  of 1.2 nm, annealed at 250 °C in FG. (c)  $I_D - V_{GS}$  and (d)  $I_D - V_{DS}$  characteristics of an  $\text{In}_2\text{O}_3$  transistor with  $L_{ch}$  of 40 nm and  $T_{ch}$  of 1.2 nm, annealed at 350 °C in N<sub>2</sub>. (e)  $I_D - V_{GS}$  and (f)  $I_D - V_{DS}$  characteristics of an  $\text{In}_2\text{O}_3$  transistor with  $L_{ch}$  of 40 nm and  $T_{ch}$  of 1.2 nm, annealed at 350 °C in O<sub>2</sub>.

impact from contact resistance  $R_C$ , which is generally low at back-gate  $\text{In}_2\text{O}_3$  transistors studied here. The intrinsic mobility of annealed ALD  $\text{In}_2\text{O}_3$  can be even higher. The devices exhibit excellent immunity to short channel effects down to 40 nm because of the ultrathin  $\text{In}_2\text{O}_3$  channel and scaled EOT.

To understand the physics and chemistry of annealing effects on ALD  $\text{In}_2\text{O}_3$  transistors, a systematic annealing study was conducted at various temperatures from 250 °C to 350 °C in N<sub>2</sub>, O<sub>2</sub>, and FG environments. Such annealing study was done on  $\text{In}_2\text{O}_3$  with a thinner channel with  $T_{ch}$  of 1.2 nm, because  $\text{In}_2\text{O}_3$  transistors with  $T_{ch}$  of 1.2 nm have a  $V_T$  near zero, so that both carrier density enhancement and reduction can be captured.

Fig. 3 shows representative  $I - V$  results of short channel ALD  $\text{In}_2\text{O}_3$  transistors with  $T_{ch}$  of 1.2 nm after annealing. Fig. 3(a) and (b) shows the  $I_D - V_{GS}$  and  $I_D - V_{DS}$  characteristics of an  $\text{In}_2\text{O}_3$  transistor with  $L_{ch}$  of 40 nm and  $T_{ch}$  of 1.2 nm, with 250 °C annealing in FG. Maximum  $I_D$  of 1.3 A/mm is achieved at  $V_{DS}$  of 0.6 V with  $V_T$  of 0.01 V. Fig. 3(c) and (d) shows the  $I_D - V_{GS}$  and  $I_D - V_{DS}$  characteristics of an  $\text{In}_2\text{O}_3$  transistor with  $L_{ch}$  of 40 nm and  $T_{ch}$  of 1.2 nm, with 350 °C annealing in N<sub>2</sub>. Maximum  $I_D$  of 1.4 A/mm is achieved at  $V_{DS}$  of 1 V with  $V_T$  of 0.7 V. Fig. 3(e) and (f) shows the  $I_D - V_{GS}$  and  $I_D - V_{DS}$  characteristics of an  $\text{In}_2\text{O}_3$  transistor with  $L_{ch}$  of 40 nm and  $T_{ch}$  of 1.2 nm, with 350 °C annealing in O<sub>2</sub>. Maximum  $I_D$  of 1.3 A/mm is achieved at  $V_{DS}$  of 1 V with  $V_T$  of 0.5 V.



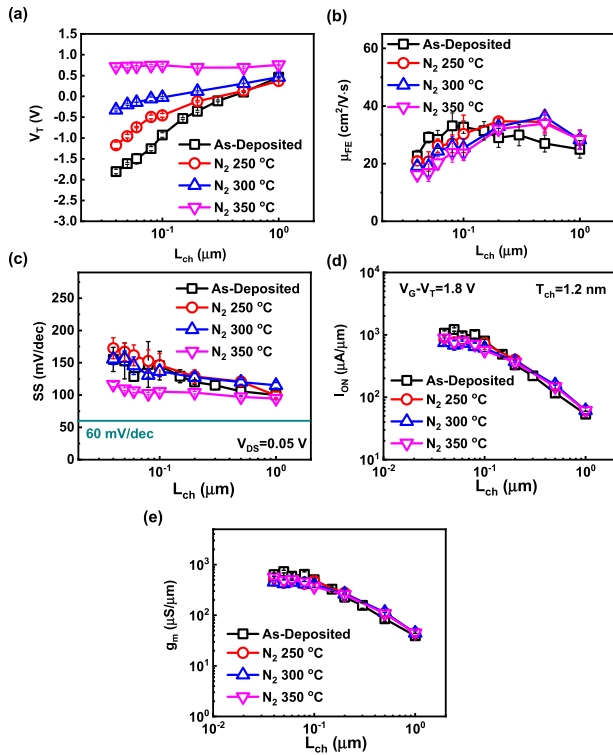


**Fig. 4.** (a)  $V_T$ , (b)  $\mu_{FE}$ , (c) SS, (d)  $I_{on}$ , and (e)  $g_m$  scaling metrics of  $\text{In}_2\text{O}_3$  transistors with  $L_{ch}$  from  $1 \mu\text{m}$  to  $40 \text{ nm}$  and  $T_{ch}$  of  $1.2 \text{ nm}$ . The devices were annealing from  $250 \text{ }^\circ\text{C}$  to  $350 \text{ }^\circ\text{C}$  in  $\text{N}_2$  and compared to devices without annealing.  $I_{on}$  and  $g_m$  are extracted at  $V_{DS} = 1 \text{ V}$  unless otherwise specified.  $I_{on}$  and  $g_m$  at  $L_{ch}$  of  $80, 60, 50,$  and  $40 \text{ nm}$  annealed at  $250 \text{ }^\circ\text{C}$  and  $300 \text{ }^\circ\text{C}$  are extracted at  $V_{DS}$  of  $0.8, 0.7, 0.7, 0.6 \text{ V}$ . Lower voltage at shorter channel devices are used to avoid the impact of self-heating on devices. Each data point represents the average of at least 5 devices.

**Fig. 4** summarizes the scaling metrics of  $\text{In}_2\text{O}_3$  transistors with  $L_{ch}$  from  $1 \mu\text{m}$  down to  $40 \text{ nm}$  and with  $T_{ch}$  of  $1.2 \text{ nm}$ , annealed from  $250 \text{ }^\circ\text{C}$  to  $350 \text{ }^\circ\text{C}$  in  $\text{N}_2$  and compared to devices without annealing. **Fig. 4(a)** studies the impact of  $\text{N}_2$  annealing at different temperatures on  $V_T$ , showing a large positive  $V_T$  shift by annealing in  $\text{N}_2$ . Note that the as-deposited  $\text{In}_2\text{O}_3$  transistors have a clearly  $L_{ch}$  dependent  $V_T$  even in long channel devices, which is not predicted by semiconductor device physics.  $V_T$  has negligible  $L_{ch}$  dependence after  $\text{N}_2$  annealing at  $350 \text{ }^\circ\text{C}$ , suggesting such  $V_T$  dependence is from the defects introduced in device fabrication and these defects are completely removed, as also discussed previously. **Fig. 4(b)** illustrates the impact of  $\text{N}_2$  annealing on extrinsic  $\mu_{FE}$  extracted from the extrinsic  $g_m$  without considering the contact resistance.  $\mu_{FE}$  increases after annealing at the long channel but  $\mu_{FE}$  decreases after annealing at short channel, indicating the mobility is enhanced by  $\text{N}_2$  annealing but  $R_C$  increases due to the reduction of carrier density. Extracted  $\mu_{FE}$  of  $\text{In}_2\text{O}_3$  with  $\text{N}_2$  annealing at  $350 \text{ }^\circ\text{C}$  will decrease at the short-channel devices, because the  $V_T$  shift at short channel by annealing, leading to very different contact resistance due to the different carrier concentration. The extracted  $\mu_{FE}$  should only be regarded as the lower limit of the intrinsic mobility of the  $\text{In}_2\text{O}_3$  film. **Fig. 4(c)** presents the SS versus  $L_{ch}$  characteristics at  $V_{DS}$  of  $0.05 \text{ V}$  at different  $\text{N}_2$  annealing

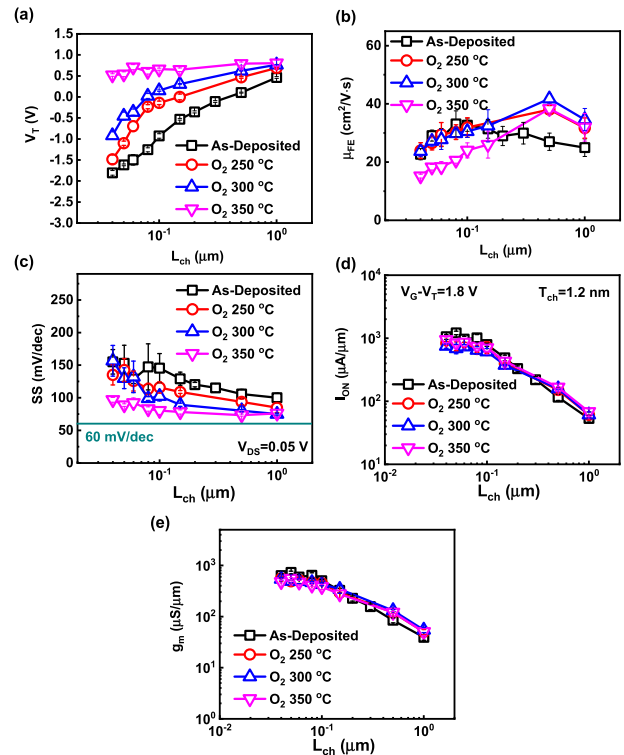


**Fig. 5.** (a)  $V_T$ , (b)  $\mu_{FE}$ , (c) SS, (d)  $I_{on}$ , and (e)  $g_m$  scaling metrics of  $\text{In}_2\text{O}_3$  transistors with  $L_{ch}$  from  $1 \mu\text{m}$  to  $40 \text{ nm}$  and  $T_{ch}$  of  $1.2 \text{ nm}$ . The devices were annealing from  $250 \text{ }^\circ\text{C}$  to  $350 \text{ }^\circ\text{C}$  in  $\text{O}_2$  and compared to devices without annealing.  $I_{on}$  and  $g_m$  are extracted at  $V_{DS} = 1 \text{ V}$  unless otherwise specified.  $I_{on}$  and  $g_m$  at  $L_{ch}$  of  $100, 80, 60, 50$  and  $40 \text{ nm}$  annealed at  $250 \text{ }^\circ\text{C}$  and  $300 \text{ }^\circ\text{C}$  are extracted at  $V_{DS}$  of  $0.9, 0.8, 0.7, 0.6, 0.6 \text{ V}$ .  $I_{on}$  and  $g_m$  at  $L_{ch}$  of  $40 \text{ nm}$  annealed at  $350 \text{ }^\circ\text{C}$  are extracted at  $V_{DS}$  of  $0.8 \text{ V}$ . Lower voltage at shorter channel devices are used to avoid the impact of self-heating on devices. Each data point represents the average of at least 5 devices.

temperatures. Minimum SS of  $97.0 \text{ mV/dec}$  is achieved. SS is found to decrease with increasing  $\text{N}_2$  annealing temperature, suggesting  $D_{it}$  can be reduced effectively by  $\text{N}_2$  annealing. **Fig. 4(d)** and **(f)** shows the ON-current ( $I_{on}$ ) at  $V_{GS}-V_T = 1.8 \text{ V}$  and transconductance ( $g_m$ ) versus  $L_{ch}$  characteristics.  $I_{on}$  and  $g_m$  are extracted at  $V_{DS} = 1 \text{ V}$  unless otherwise specified. Lower voltage at shorter channel devices are used to avoid the impact of self-heating on devices since self-heating may induce a similar effect as annealing, as specified in **Fig. 4** caption.

**Fig. 5** summarizes the scaling metrics of  $\text{In}_2\text{O}_3$  transistors with  $L_{ch}$  from  $1 \mu\text{m}$  down to  $40 \text{ nm}$  and with  $T_{ch}$  of  $1.2 \text{ nm}$ , annealed from  $250 \text{ }^\circ\text{C}$  to  $350 \text{ }^\circ\text{C}$  in  $\text{O}_2$  and compared to devices without annealing. Minimum SS of  $73.0 \text{ mV/dec}$  is achieved after  $350 \text{ }^\circ\text{C}$  annealing in  $\text{O}_2$ , suggesting  $\text{O}_2$  annealing can more effectively reduce  $D_{it}$  than  $\text{N}_2$  annealing. Except for the significantly reduced SS, other device performance criteria from devices by  $\text{O}_2$  annealing and  $\text{N}_2$  annealing are pretty much similar and follow the same trend.

**Fig. 6** summarizes the scaling metrics of  $\text{In}_2\text{O}_3$  transistors with  $L_{ch}$  from  $1 \mu\text{m}$  down to  $40 \text{ nm}$  and with  $T_{ch}$  of  $1.2 \text{ nm}$ , annealed from  $250 \text{ }^\circ\text{C}$  to  $350 \text{ }^\circ\text{C}$  in FG and compared to devices without annealing. **Fig. 6(a)** shows the  $I_D-V_{GS}$  characteristics of an  $\text{In}_2\text{O}_3$  transistor with  $L_{ch}$  of  $400 \text{ nm}$  and  $T_{ch}$

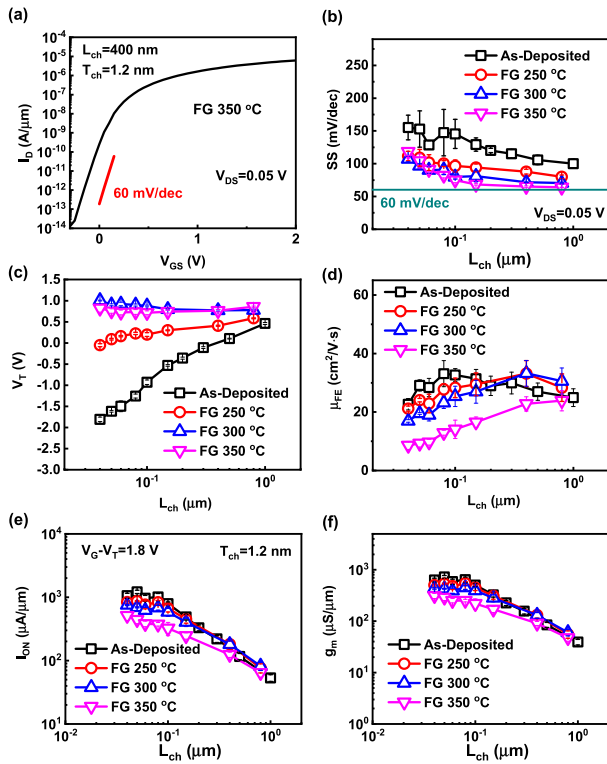


**Fig. 6.** (a)  $I_D$ - $V_{GS}$  characteristics of an  $\text{In}_2\text{O}_3$  transistor with  $L_{ch}$  of 400 nm and  $T_{ch}$  of 1.2 nm at  $V_{DS}$  of 0.05 V, annealed at 350 °C in FG. (b) SS, (c)  $V_T$ , (d)  $\mu_{FE}$ , (e)  $I_{on}$ , and (f)  $g_m$  scaling metrics of  $\text{In}_2\text{O}_3$  transistors with  $L_{ch}$  from 1  $\mu\text{m}$  to 40 nm and  $T_{ch}$  of 1.2 nm. The devices were annealed from 250 °C to 350 °C in FG and compared to devices without annealing.  $I_{on}$  and  $g_m$  are extracted at  $V_{DS} = 1$  V unless otherwise specified.  $I_{on}$  and  $g_m$  at  $L_{ch}$  of 60, 50 and 40 nm annealed at 300 °C are extracted at  $V_{DS}$  of 0.8, 0.7, 0.7 V.  $I_{on}$  and  $g_m$  at  $L_{ch}$  of 60, 50, and 40 nm annealed at 250 °C are extracted at  $V_{DS}$  of 0.8, 0.7, 0.6 V. Lower voltage at shorter channel devices are used to avoid the impact of self-heating on devices. Each data point represents the average of at least 5 devices.

of 1.2 nm at  $V_{DS}$  of 0.05 V, with 350 °C annealing in FG, exhibiting a *nearly ideal* SS. Fig. 6(b) presents the SS versus  $L_{ch}$  characteristics at  $V_{DS}$  of 0.05 V at different FG annealing temperatures. Minimum SS of 63.8 mV/dec (average value) is achieved by FG annealing at 350 °C, corresponding to a low  $D_{it}$  of  $6.3 \times 10^{11} \text{ cm}^{-2} \cdot \text{eV}^{-1}$ , extracted from subthreshold method. It suggests that hydrogen is the most effective way to passivate the interface traps in this  $\text{HfO}_2/\text{In}_2\text{O}_3$  material system. Other device performance criteria from devices by FG annealing follow the similar trend to  $\text{O}_2$  and  $\text{N}_2$  annealing, suggesting the  $V_T$  shift by annealing is the result of annealing temperature instead of the annealing environments.

Oxygen vacancies are known to act as shallow donors and determine the carrier density in doped- $\text{In}_2\text{O}_3$  [19]. It is widely reported that the oxygen pressure during film sputter deposition and thermal annealing have significant impact on the electrical conductivity of doped- $\text{In}_2\text{O}_3$  films such as IGZO and indium-tin-oxide (ITO) [1], [5], [19]–[21]. It was understood that oxygen vacancies form both a deep localized state and a shallow donor state depending on local atomic configurations by first principle simulation [17], [22]. Therefore, because of the similarity between ALD  $\text{In}_2\text{O}_3$  and doped- $\text{In}_2\text{O}_3$ , it is assumed that oxygen vacancies are also shallow donors in ALD  $\text{In}_2\text{O}_3$  films, such assumption may need further

verification by materials analysis and simulation. Based on this assumption, it is speculated that the  $V_T$  shift of ALD  $\text{In}_2\text{O}_3$  transistors by annealing is likely to be the result of oxidation of oxygen deficiencies or vacancies by excessive oxygen inside the  $\text{In}_2\text{O}_3$  film not from the environment because FG,  $\text{N}_2$  and  $\text{O}_2$  annealing give similar results. The excessive oxygen is likely to come from ALD or other processes during device fabrication. The ALD temperature is not high enough for these excessive oxygens to oxidize the oxygen vacancies, as more than 300 °C is needed to annihilate these defects.

Annealing at 350 °C in all environments causes the slight deteriorate of  $\mu_{FE}$ , most likely due to the degradation of  $\text{Ni}/\text{In}_2\text{O}_3$  contact resistance because of the reduction of carrier density, which may be further improved by introducing conducting oxide contact such as ITO [5], [6].

As can be clearly seen from Figs. 4–6, devices after 350 °C annealing in  $\text{O}_2$ ,  $\text{N}_2$ , and FG show similar  $V_T$ , suggesting the ALD  $\text{In}_2\text{O}_3$  is less affected by the widely exhibiting hydrogen doping issue in IGZO [16], [18], [23]–[25]. This result also indicates that the role of hydrogen in ALD  $\text{In}_2\text{O}_3$  may be different from the hydrogen in sputter IGZO films. This is a strong support that ALD  $\text{In}_2\text{O}_3$  can be highly compatible with hydrogen-rich environment in CMOS BEOL processes.

The detailed surface chemistry experiments and the complete understanding of the hydrogen chemistry in ALD  $\text{In}_2\text{O}_3$  are out of the scope of this article. We may give the following two hypotheses to explain the experimental phenomenon. First, all the oxygen bonds in bulk ALD  $\text{In}_2\text{O}_3$  film may be already passivated by the hydrogen from water precursors, in a hydrogen saturation state. Thus, new hydrogen from the environment has little impact on the doping of ALD  $\text{In}_2\text{O}_3$  film. Second, hydrogen may not behave like shallow dopant in ALD  $\text{In}_2\text{O}_3$  due to the possible different electronic structures. As the first work on high-performance enhancement-mode  $\text{In}_2\text{O}_3$  transistors with different annealing conditions, we wish it can inspire more fundamental studies on surface chemistry and physics research on this novel material system.

The reliability performance of devices is critical for the application of the ALD  $\text{In}_2\text{O}_3$  technology. A complete understanding and optimization on reliability performance is still required to qualify the ALD  $\text{In}_2\text{O}_3$  technology for CMOS BEOL transistors for monolithic 3-D integration.

#### IV. CONCLUSION

In summary, the impact of post-deposition annealing in various environments, such as  $\text{O}_2$ ,  $\text{N}_2$ , and FG (96%  $\text{N}_2/4\% \text{H}_2$ ), at various BEOL compatible low temperatures on ALD  $\text{In}_2\text{O}_3$  transistors is systematically studied. The optimized annealing conditions are found to enhance the performance of  $\text{In}_2\text{O}_3$  transistors significantly. Enhancement-mode  $\text{In}_2\text{O}_3$  transistors with record high drain current of 2.2 A/mm at  $V_{DS}$  of 0.7 V with  $V_T$  of 0.02 V are demonstrated. SS as low as 63.8 mV/dec is achieved, corresponding to a low  $D_{it}$  of  $6.3 \times 10^{11} \text{ cm}^{-2} \cdot \text{eV}^{-1}$ . The physical origin of the positive threshold voltage shift by annealing is speculated as the passivation of oxygen vacancies by excessive oxygen in as-deposited films. Remarkably, the ALD  $\text{In}_2\text{O}_3$  devices are found to be stable in hydrogen environment, being less

affected by the well-known hydrogen doping issue in IGZO. Therefore, ALD  $\text{In}_2\text{O}_3$  transistors and its high compatibility with hydrogen-rich CMOS BEOL process suggest ALD  $\text{In}_2\text{O}_3$  is the promising channel material for BEOL compatible transistors toward monolithic 3-D integration.

## REFERENCES

- [1] K. Nomura, A. Takagi, T. Kamiya, H. Ohta, M. Hirano, and H. Hosono, "Amorphous oxide semiconductors for high-performance flexible thin-film transistors," *Jpn. J. Appl. Phys.*, vol. 45, no. 5B, pp. 4303–4308, May 2006, doi: [10.1143/JJAP.45.4303](https://doi.org/10.1143/JJAP.45.4303).
- [2] T. Kamiya, K. Nomura, and H. Hosono, "Present status of amorphous In–Ga–Zn–O thin-film transistors," *Sci. Technol. Adv. Mater.*, vol. 11, no. 4, Feb. 2010, Art. no. 044305, doi: [10.1088/1468-6996/11/4/044305](https://doi.org/10.1088/1468-6996/11/4/044305).
- [3] M. Si *et al.*, "Why  $\text{In}_2\text{O}_3$  can make 0.7 nm atomic layer thin transistors," *Nano Lett.*, vol. 21, no. 4, pp. 500–506, Jan. 2021, doi: [10.1021/acs.nanolett.0c03967](https://doi.org/10.1021/acs.nanolett.0c03967).
- [4] M. Si, Z. Lin, A. Charnas, and P. D. Ye, "Scaled atomic-layer-deposited indium oxide nanometer transistors with maximum drain current exceeding 2 A/mm at drain voltage of 0.7 V," *IEEE Electron Device Lett.*, early access, Dec. 9, 2020, doi: [10.1109/LED.2020.3043430](https://doi.org/10.1109/LED.2020.3043430).
- [5] S. Li *et al.*, "Nanometre-thin indium tin oxide for advanced high-performance electronics," *Nature Mater.*, vol. 18, no. 10, pp. 1091–1097, Oct. 2019, doi: [10.1038/s41563-019-0455-8](https://doi.org/10.1038/s41563-019-0455-8).
- [6] M. Si *et al.*, "Indium–tin-oxide transistors with one nanometer thick channel and ferroelectric gating," *ACS Nano*, vol. 14, no. 9, pp. 11542–11547, Sep. 2020, doi: [10.1021/acsnano.0c03978](https://doi.org/10.1021/acsnano.0c03978).
- [7] W. Chakraborty, B. Grisafe, H. Ye, I. Lightcap, K. Ni, and S. Datta, "BEOL compatible dual-gate ultra thin-body W-doped indium-oxide transistor with  $I_{on} = 370 \mu\text{A}/\mu\text{m}$ ,  $SS = 73 \text{ mV/dec}$  and  $I_{on}/I_{off}$  ratio  $> 4 \times 10^9$ ," in *Proc. IEEE Symp. VLSI Technol.*, Jun. 2020, pp. 1–2, Paper TH2.1.
- [8] H. Fujiwara, Y. Sato, N. Saito, T. Ueda, and K. Ikeda, "Surrounding gate vertical-channel FET with gate length of 40 nm using BEOL compatible high-thermal-tolerance In–Al–Zn oxide channel," in *Proc. IEEE Symp. VLSI Technol.*, Jun. 2020, pp. 1–2, Paper TH2.2.
- [9] J. Wu, F. Mo, T. Saraya, T. Hiramoto, and M. Kobayashi, "A monolithic 3D integration of RRAM array with oxide semiconductor FET for in-memory computing in quantized neural network AI applications," in *Proc. IEEE Symp. VLSI Technol.*, Jun. 2020, pp. 1–2, Paper THL.4.
- [10] S. Samanta, K. Han, C. Sun, C. Wang, A. V.-Y. Thean, and X. Gong, "Amorphous IGZO TFTs featuring extremely-scaled channel thickness and 38 nm channel length: Achieving record high  $G_{m,max}$  of  $125 \mu\text{S}/\mu\text{m}$  at  $V_{DS}$  of 1 V and  $I_{ON}$  of  $350 \mu\text{A}/\mu\text{m}$ ," in *Proc. Symp. VLSI Technol.*, Jun. 2020, pp. 1–2, Paper TH2.1.
- [11] H. Y. Kim *et al.*, "Low-temperature growth of indium oxide thin film by plasma-enhanced atomic layer deposition using liquid dimethyl(*N*-ethoxy-2,2-dimethylpropanamido) indium for high-mobility thin film transistor application," *ACS Appl. Mater. Interfaces*, vol. 8, no. 40, pp. 26924–26931, 2016, doi: [10.1021/acsami.6b07332](https://doi.org/10.1021/acsami.6b07332).
- [12] H.-I. Yeom, J. B. Ko, G. Mun, and S.-H.-K. Park, "High mobility polycrystalline indium oxide thin-film transistors by means of plasma-enhanced atomic layer deposition," *J. Mater. Chem. C*, vol. 4, no. 28, pp. 6873–6880, 2016, doi: [10.1039/c6tc00580b](https://doi.org/10.1039/c6tc00580b).
- [13] J. Lee *et al.*, "High mobility ultra-thin crystalline indium oxide thin film transistor using atomic layer deposition," *Appl. Phys. Lett.*, vol. 113, no. 11, Sep. 2018, Art. no. 112102, doi: [10.1063/1.5041029](https://doi.org/10.1063/1.5041029).
- [14] Q. Ma *et al.*, "Atomic-layer-deposition of indium oxide nano-films for thin-film transistors," *Nanoscale Res. Lett.*, vol. 13, no. 1, p. 4, Dec. 2018, doi: [10.1186/s11671-017-2414-0](https://doi.org/10.1186/s11671-017-2414-0).
- [15] Y. Kumura *et al.*, "A  $\text{SrRuO}_3/\text{IrO}_2$  top electrode FeRAM with Cu BEOL process for embedded memory of 130 nm generation and beyond," *Solid-State Electron.*, vol. 50, no. 4, pp. 606–612, Apr. 2006, doi: [10.1016/j.sse.2006.03.015](https://doi.org/10.1016/j.sse.2006.03.015).
- [16] T. Kamiya, K. Nomura, and H. Hosono, "Origins of high mobility and low operation voltage of amorphous oxide TFTs: Electronic structure, electron transport, defects and doping," *J. Display Technol.*, vol. 5, no. 12, pp. 468–483, 2009, doi: [10.1109/JDT.2009.2034559](https://doi.org/10.1109/JDT.2009.2034559).
- [17] T. Kamiya, K. Nomura, and H. Hosono, "Subgap states, doping and defect formation energies in amorphous oxide semiconductor a-InGaZnO<sub>4</sub> studied by density functional theory," *Phys. Status Solidi A*, vol. 207, no. 7, pp. 1698–1703, May 2010, doi: [10.1002/pssa.200983772](https://doi.org/10.1002/pssa.200983772).
- [18] T. Kamiya and H. Hosono, "(Invited) roles of hydrogen in amorphous oxide semiconductor," *ECS Trans.*, vol. 54, no. 1, pp. 103–113, Jun. 2013, doi: [10.1149/05401.0103ecst](https://doi.org/10.1149/05401.0103ecst).
- [19] T. Kamiya and H. Hosono, "Material characteristics and applications of transparent amorphous oxide semiconductors," *NPG Asia Mater.*, vol. 2, no. 1, pp. 15–22, Jan. 2010, doi: [10.1038/asiamat.2010.5](https://doi.org/10.1038/asiamat.2010.5).
- [20] H. Yabuta *et al.*, "High-mobility thin-film transistor with amorphous InGaZnO<sub>4</sub> channel fabricated by room temperature RF-magnetron sputtering," *Appl. Phys. Lett.*, vol. 89, no. 11, Sep. 2006, Art. no. 112123, doi: [10.1063/1.2353811](https://doi.org/10.1063/1.2353811).
- [21] H. Kim *et al.*, "Indium tin oxide thin films for organic light-emitting devices," *Appl. Phys. Lett.*, vol. 74, no. 23, pp. 3444–3446, Jun. 1999, doi: [10.1063/1.124122](https://doi.org/10.1063/1.124122).
- [22] T. Kamiya, K. Nomura, and H. Hosono, "Electronic structure of the amorphous oxide semiconductor a-InGaZnO<sub>4-x</sub>: Tauc-Lorentz optical model and origins of subgap states," *Phys. Status Solidi A*, vol. 206, no. 5, pp. 860–867, 2009, doi: [10.1002/pssa.200881303](https://doi.org/10.1002/pssa.200881303).
- [23] A. Sato *et al.*, "Amorphous In–Ga–Zn–O coplanar homojunction thin-film transistor," *Appl. Phys. Lett.*, vol. 94, no. 13, Mar. 2009, Art. no. 133502, doi: [10.1063/1.3112566](https://doi.org/10.1063/1.3112566).
- [24] H. Kumomi *et al.*, "Materials, devices, and circuits of transparent amorphous-oxide semiconductor," *J. Display Technol.*, vol. 5, no. 12, pp. 531–540, Dec. 2009, doi: [10.1109/JDT.2009.2025521](https://doi.org/10.1109/JDT.2009.2025521).
- [25] L. Shao, K. Nomura, T. Kamiya, and H. Hosono, "Operation characteristics of thin-film transistors using very thin amorphous In–Ga–Zn–O channels," *Electrochem. Solid-State Lett.*, vol. 14, no. 5, p. H197, 2011, doi: [10.1149/1.3555070](https://doi.org/10.1149/1.3555070).